Wear 338-339 (2015) 394–405

Contents lists available at ScienceDirect

Wear

journal homepage: www.elsevier.com/locate/wear

Effects of fatigue damage and wear on fretting fatigue under partial slip condition

Fei Shen [a], Weiping Hu [a,b,*,1], George Z. Voyiadjis [b], Qingchun Meng [a]

[a] Institute of Solid Mechanics, School of Aeronautics Science and Engineering, Beihang University, Beijing 100191, China
[b] Department of Civil and Environmental Engineering, Louisiana State University, Baton Rouge, LA 70803, USA

ARTICLE INFO

Article history:
Received 3 May 2015
Received in revised form
22 July 2015
Accepted 24 July 2015
Available online 1 August 2015

Keywords:
Fretting fatigue
Damage mechanics
Finite element modeling
Ti–6Al–4V

ABSTRACT

The continuum damage mechanics model incorporating wear was developed in the previous paper by the authors [27] to predict the fretting fatigue crack initiation life for both cases of partial slip and gross sliding. In the present study, the effects of external parameters on the fretting fatigue crack initiation behaviour under partial slip condition are investigated systematically. Firstly, a different fatigue damage accumulation rule is used, which can predict a more reasonable damage process. Secondly, the effects of the relative slip amplitude and wear coefficient are evaluated based on the improved approach. It is significant to note that the impact of wear coefficient on the fretting fatigue life is non-monotonic, and the action mechanism of that is analysed in detail in this work. Finally, the combination and competition between fatigue damage and wear are presented. The results indicate that none of the fatigue damage and wear can be neglected in the fretting fatigue life prediction.

© 2015 Elsevier B.V. All rights reserved.

1. Introduction

Fretting fatigue is a process of damage accumulation that occurs when two bodies in contact experience small reciprocating motion. Depending on the relative slip status between the two contacting bodies, fretting fatigue can be classified into two different regimes: the partial slip regime and the gross sliding regime. In the partial slip case, relative slip only occurs in the portions of the contact zone and mainly results in crack nucleation. In the gross sliding case, all the contact surfaces experience relative slip and the main form of fretting damage is wear. The behaviors of the above fretting failure forms were widely investigated in the past decades.

Numerous efforts were undertaken to understand the behavior of fretting crack nucleation. The critical plane method based on the multi-axial fatigue model is widely used to predict the fretting fatigue crack initiation life, which looks for the maximum value of a predefined fatigue damage parameter over a number of planes and predicts the crack initiation life based on that maximum value. The location and orientation of the fretting fatigue crack are also obtained using the critical plane method [1–4]. Vázquez et al. [5] combined the finite element simulation and the critical plane method to investigate the effect of a textured surface on fretting fatigue. With the improved understanding of the behavior of fretting fatigue, further attention was devoted to the role of wear on the fretting fatigue. Two kinds of wear models, the Archard wear model and the energy wear model, were proposed by Archard [6] and Fouvry et al. [7] respectively to describe the wear mechanisms. Zeise et al. [8] proposed a novel comprehensive modeling approach to simulate the complex fretting wear process of assemblies including abrasion, corrosion, accumulation and transport of the produced debris during dynamic loading. The effect of wear is then combined with the critical plane method to predict the behavior of fretting fatigue crack initiation [9–12]. Recently, the effect of surface wear was investigated by the fretting-fatigue map concept [13] which was used to predict the crack nucleation and crack arrest boundaries [14]. However, there are two modelling simplifications in the critical plane approaches that need improvement. The first one is the Miner–Palmgren rule based on the accumulated fatigue damage, which ignores the effect of the loading sequence. The other one is the fatigue damage that is computed independently according to the stress and strain fields without accounting for the effect of fatigue damage on the stress and strain fields.

Actually, Fretting fatigue life consists of crack nucleation life and the crack propagation life. These two issues often need to be separately modelled, as in the literature [15–19]. An important aspect of the “nucleation-propagation” method is the initial crack length for the propagation period. It is difficult to define the

* Corresponding author at: Institute of Solid Mechanics, School of A eronautics Science and Engineering, Beihang University, Beijing 100191, China.
Tel.: +861082338489.
E-mail address: huweiping@buaa.edu.cn (W. Hu).
[1] Postal address: Room D604, New Main Building, 37th Xueyuan Road, Beihang University, Beijing, 100191, China

http://dx.doi.org/10.1016/j.wear.2015.07.012
0043-1648/© 2015 Elsevier B.V. All rights reserved.

macroscopic crack length, which is dependent on several factors. In the macroscopic approaches, such as the critical plane method, 10 μm is a common used value for Ti–6Al–4V [15], which means that the crack length is about 10 μm after the crack nucleation. In the work of McCarthy et al. [18,19], the micro-mechanical approach was used and a shorter initial crack with the length of 1.2 μm was used for 316 L SS. However, for some cases the crack propagation life is very short comparing to the crack nucleation life, in which the crack propagation can be neglected. This paper focuses on the crack initiation behavior of fretting fatigue, which means the research is mainly fit for the cases when the crack initiation life is the majority of the entire fatigue life.

The continuum damage mechanics (CDM) approach has been introduced in the fretting fatigue problem. A damage variable is defined as a measurement of micro-cracks and micro-voids in the material. The approach deals with the mechanical behaviour of a deteriorated medium at the macroscopic scale and evaluates progressive damage based on the damage evolution law derived from thermodynamics until damage reaches a certain critical value. Many CDM approaches have been used for the fretting fatigue problem, including uncoupled CDM approach [16,17,20], coupled CDM approach [21], and coupled CDM approach with micro-structural characterization [22]. However, the effect of wear, which is less severe than that in the gross sliding case but still exists in the partial slip case [23–26], is ignored. In the previous paper by Shen et al. [27], a coupled CDM approach with consideration of wear was developed to predict the fretting fatigue crack initiation life for both cases partial slip and gross sliding. The damage coupled Chaboche plasticity model and a combined fatigue damage model are implemented in the approach. Besides, the progressive change of the contact geometry caused by wear was considered by using the energy wear model [7] in which a constant wear coefficient was specified. The results of the literature [27] agree well with the experimental data. However, two aspects are worth studying further as outlined below.

On the one hand, in the literature [27], the total fatigue damage is the sum of two components, the elastic damage caused by the cyclic stress and the plastic damage due to the plastic strain during each cycle. The accumulation method of fatigue damage gives reasonable prediction of the fretting fatigue life. However, a limitation of the method is that it is inappropriate for the cases with large plastic deformation. For such cases, the accumulation of fatigue damage is overestimated, resulting in significant error for the prediction of the fatigue life. Since higher wear coefficient is employed in this study compared to the literature [27], plastic strain induced by wear will be greater. A more general method was employed to investigate the fatigue damage evolution of notched specimens [28], in which the total fatigue damage is the greater one of the two components. Based on the similarity of the mechanical behaviour at the notch tip and the critical contact position such as the contact edge (the edge of whole contact zone) or the stick-slip interface (the interface between the central stick zone and outside slip zones), the improved accumulation method is adopted to predict the fatigue damage evolution of fretting fatigue.

On the other hand, the effects of external parameters, including relative slip amplitude and wear coefficient, to the fretting fatigue crack initiation behaviour under the partial slip condition need to be investigated systematically using numerical implementation. The effect of the relative slip amplitude was studied experimentally by Jin and Mall [29]. The fretting fatigue life decreases in the partial slip regime but increases significantly in the gross sliding regime as the applied relative slip amplitude increases. Numerical simulations were carried out by combining the wear model and the critical plane method to describe the effect on the fretting fatigue life in the literature by Ding et al. [30] and Madge et al. [10]. However, the effect on the contact stress and subsurface stress was discussed without consideration of the fatigue damage. Wear coefficient is the other important parameter influencing the fretting fatigue life. In these numerical investigations, the wear coefficient used in the wear model was usually determined based on the wear experiments. However, the conditions of the fretting fatigue simulated numerically do not match exactly with the wear experiments, such as the heat treatment of materials or the level of loading. Thus it is necessary to identify the sensitivity of the fatigue life to the wear coefficient. In this study, the effects of the relative slip amplitude and wear coefficient to the fretting fatigue crack initiation behaviour are investigated numerically by the coupled CDM approach with consideration of the fatigue damage and wear, in which a series of slip amplitudes and several wear coefficients are employed.

Besides, the competition between the fatigue damage and wear are described empirically according to the failure form of the fretting fatigue [10]. When the contact status changes from the partial slip to the gross sliding, the corresponding failure form also changes, from the initiation of fretting fatigue crack to the wear of the contact components. In this study, a more detailed description is studied using the evolution of the contact stress and subsurface stress along the contact surface which are affected by both the fatigue damage and wear.

In the present study, a different method of fatigue damage accumulation is employed to investigate the fretting fatigue crack initiation behaviour under the partial slip condition. The effects of the relative slip amplitude and wear coefficient are evaluated based on the improved approach. The progressive evolution of the fatigue damage and wear scar are simulated under several simulation conditions including five relative slip amplitudes and four wear coefficients. The combination and competition mechanism of fatigue damage and wear to the fatigue life is also identified.

2. Theoretical models

The coupled CDM approach includes three types of theoretical models: damage coupled constitutive model, fatigue damage model and wear model, which are briefly described in this section.

2.1. Damage coupled Chaboche plasticity model

Damage mechanics based model in solid materials is the creation and growth of micro-voids or micro-cracks which are discontinuities in a medium considered as continuous at a larger scale. A damage variable is introduced to estimate the progressive deterioration of the material due to fatigue loading. In this study the case of isotropic damage is assumed with a scalar damage variable D. Strictly speaking, fatigue damage is anisotropic even for the initial isotropic materials. However, in the framework of CDM, anisotropic damage models [31–33] are much more difficult to be adopted in the fatigue damage analysis due to the inconvenience in parameter calibration, the complexity of fatigue damage evolution and the huge time requirement for calculations. Therefore, the assumption of isotropic damage is still adopted for an approximation of the real situation, which can also provide an acceptable predicted result of fretting fatigue life [20,22].

In fretting fatigue, the elasto-plastic constitutive model is more appropriate to use as one calculates the stress and strain in the contact zone where plastic deformation may occur due to stress concentration. The Chaboche plasticity model [34] is adopted in this study due to its simplicity and ease of use. In the case of fatigue damage, the damage variable is coupled into the Chaboche plasticity model by using the effective stress in lieu of the stress used in the elasticity law and in the Mises yield criterion, which is based on the hypothesis of strain equivalence. The basic equations

of the damage coupled elasto-plastic constitutive model are listed below [35].

- The decomposition of the total strain for small strains is expressed by

$$\varepsilon_{ij} = \varepsilon_{ij}^{e} + \varepsilon_{ij}^{p} \tag{1}$$

where ε_{ij}^{e} and ε_{ij}^{p} are the elastic strain and plastic strain, respectively.

- The elasticity law with damage is expressed by

$$\varepsilon_{ij}^{e} = \frac{1+\nu}{E}\left(\frac{\sigma_{ij}}{1-D}\right) - \frac{\nu}{E}\left(\frac{\sigma_{kk}\delta_{ij}}{1-D}\right) \tag{2}$$

where E and ν are the elastic modulus and Poisson's ratio respectively of the undamaged material. The variable σ_{ij} is the Cauchy stress of the damaged material.

- The yield function and plastic flow with damage are respectively expressed by

$$F = \left(\frac{\sigma_{ij}}{1-D} - \alpha_{ij}\right)_{\text{eq}} - \sigma_y \tag{3}$$

$$\dot{\varepsilon}_{ij}^{p} = \dot{\lambda}\frac{\partial F}{\partial \sigma_{ij}} = \frac{3}{2}\frac{\dot{\lambda}}{1-D}\frac{\left(\frac{\sigma_{ij}}{1-D} - \alpha_{ij}\right)_{\text{dev}}}{\left(\frac{\sigma_{kl}}{1-D} - \alpha_{kl}\right)_{\text{eq}}} \tag{4}$$

and

$$\dot{p} = \sqrt{\frac{2}{3}\dot{\varepsilon}_{ij}^{p}\dot{\varepsilon}_{ij}^{p}} = \frac{\dot{\lambda}}{1-D} \tag{5}$$

The subscript 'dev' and 'eq' represent the deviatoric part of the stress and the von Mises equivalent stress, respectively. The term α_{ij} is the deviatoric component of the back stress, $\dot{\lambda}$ is the plastic multiplier and $\dot{p}$ is the accumulated plastic strain rate. The term σ_y represents the size of the yield surface which is assumed to remain unchanged in this study.

- The kinematic hardening law with damage is expressed by

$$\alpha_{ij} = \sum_{k=1}^{N} \alpha_{ij}^{(k)} \tag{6}$$

$$\dot{\alpha}_{ij}^{(k)} = (1-D)\left(\frac{2}{3}C_k\dot{\varepsilon}_{ij}^{p} - \gamma_k\alpha_{ij}^{(k)}\dot{p}\right) \tag{7}$$

where N is the number of the back stress components. Parameters C_k and γ_k are material constants obtained from experimental tests.

2.2. Fatigue damage model

Plastic deformations may occur in the contact zone due to stress concentration and wear. Using only one fatigue damage model for either the high cycle fatigue or the low cycle fatigue is inadequate to describe the evolution of fatigue damage. Therefore, two fatigue damage models are employed in this study, which are often used in the high cycle fatigue (HCF) and low cycle fatigue (LCF). In the high cycle fatigue, the evolution of fatigue damage is governed by the cyclic stress, which is expressed as follows [21,36]:

$$\frac{dD_e}{dN} = \left[1-(1-D)^{\beta+1}\right]^{1-a\left\langle\frac{A_{II}-\sigma_{l0}(1-3b_1\sigma_{H,\text{mean}})}{\sigma_u-\sigma_{\text{eq, max}}}\right\rangle} \left[\frac{A_{II}}{M_0(1-3b_2\sigma_{H,\text{mean}})(1-D)}\right]^{\beta} \tag{8}$$

where A_{II} and $\sigma_{H,\text{mean}}$ are the amplitude of the octahedral shear stress and the mean value of the hydrostatic stress in a loading cycle, respectively. The term $\sigma_{eq,\,\max}$ is the maximum equivalent stress over a loading cycle, σ_{l0} is the fatigue limit at the fully reversed loading condition, and σ_u is the ultimate tensile stress. The details for the stress-based damage model can also be obtained by referring to the literature [21,37]. The five parameters, a, M_0, β, b_1 and b_2, are determined by using fatigue test data of standard specimens. In the low cycle fatigue, the corresponding fatigue damage model is dependent on the accumulated plastic strain, which is given by [35]

$$\frac{dD_p}{dN} = \left[\frac{\left(\sigma_{\max}^{*}\right)^2}{2ES(1-D)^2}\right]^{m}\Delta p \tag{9}$$

where $\sigma_{\max}^{*}$ is the maximum value of the damage equivalent stress over a loading cycle. The parameters S and m are determined from the experimentally determined curve of plastic strain versus number of cycles to failure.

Two rates of fatigue damage can be calculated using the above two models when plastic deformation occurs. A method of fatigue damage accumulation was presented by the authors as the total rate is the sum of two rates [27]. In this study a different method is employed, which is more general for fretting fatigue and notch fatigue [28]. The larger one of the two rates is assigned as the current damage rate.

$$\frac{dD}{dN} = \max\left\{\frac{dD_e}{dN}, \frac{dD_p}{dN}\right\} \tag{10}$$

2.3. Energy wear model

The energy wear model considers the interfacial shear work as the significant wear parameter controlling the wear volume calculation. For the 2D fretting model, at time t and position x along the contact surface, the local wear depth can be expressed as follows [11]

$$h(x,t) = \phi\int_{t=0}^{t} q(x,t)\,ds(x,t) \tag{11}$$

where ϕ is the wear coefficient, $q(x,t)$ is the local shear traction and $ds(x,t)$ is the increment of local relative slip. Parameter ϕ is a critical constant determined through the wear experiment.

From Eq. (11), one sees that the effect of wear has a direct relation with the wear coefficient which should be obtained through experiments. In the literature [27], a specified wear coefficient was chosen in the numerical simulation due to lack of tests conducted by the authors. For the purpose of evaluating the effect of the wear coefficient on the wear scar and the fretting fatigue life, three wear coefficients from the published literature are adopted in this study.

3. Numerical algorithm

These three types of models mentioned above are implemented in conjunction with the finite element code ABAQUS [38] to analyze the fretting fatigue crack initiation behavior. The numerical implementation used here is similar to that in the previous paper [27] except the calculation method for the fatigue damage accumulation is different. The flowchart of the algorithm is shown in Fig. 1 and the detailed steps are presented below:

(1) The initial damage for each element is assumed to be zero.
(2) The damage coupled Chaboche constitutive equations, Eqs. (1)–(7), are solved to obtain the stress, and elastic and plastic strains. The stress and accumulated plastic strain histories are calculated for the

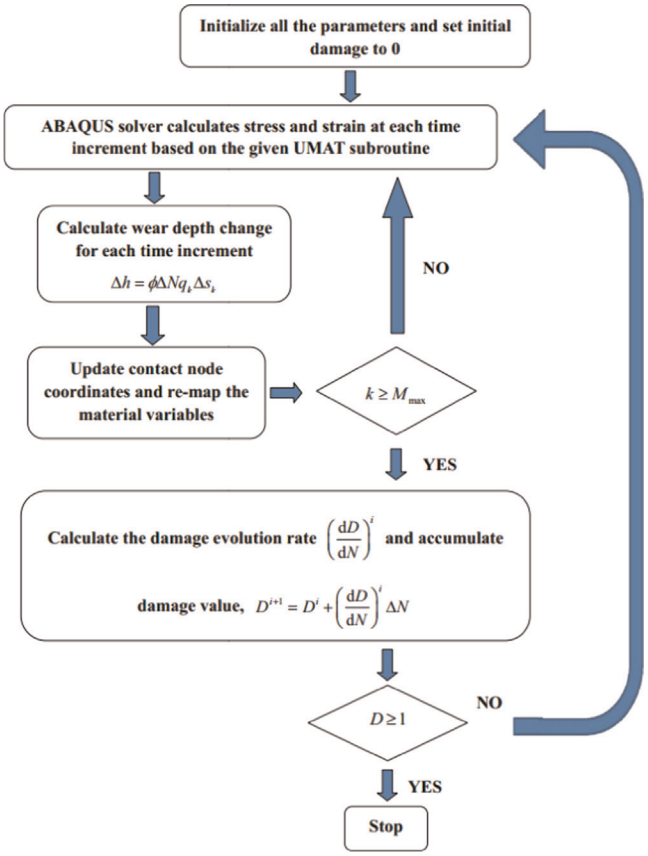

Fig. 1. Simplified flowchart of the numerical algorithm.

current block of cycles. The loading block of cycles instead of the individual loading cycle is applied in the numerical implementation due to the computationally expensive approach (prohibitive in some cases) to simulate each loading cycle. One loading block of cycles includes ΔN loading cycles. The stress, accumulated plastic strain and fatigue damage are assumed to remain unchanged in the block of cycles.

(3) During each block of cycles, three steps that are used to implement the wear model are listed below:

a. For a contact node, the increment of local wear depth at the kth time increment for a block is given as

$$\Delta h = \phi \Delta N q_k \Delta s_k \tag{12}$$

where q_k and Δs_k are shear traction and incremental slip for the kth time increment, respectively. The increment of local wear depth, Δh, is implemented by moving the surface nodes in the local normal direction at the end of each time increment.

b. The material variables are re-mapped to the new position by solving the advection equations using a second order numerical method termed the Lax-Wendroff method [38].

c. Repeat steps (a) and (b) until the number of time increment k reaches the maximum number of time increment within one fretting cycle, M_{max}. In this study, $M_{max} = 40$.

(4) After each block of cycles, the following two steps are used to update the damage value and the number of cycles. These steps are listed below:

a. According to the stress and accumulated plastic strain histories, the damage evolution rate is calculated based on Eq. (10).

$$\left(\frac{dD}{dN}\right)_j^i = \max\left\{\left(\frac{dD^e}{dN}\right)_j^i, \left(\frac{dD^p}{dN}\right)_j^i\right\} \tag{13}$$

where i represents the current block of cycles and j is the element number.

b. The damage values and the number of cycles for all elements are updated at the end of the current block of cycles.

$$D_j^{i+1} = D_j^i + \left(\frac{dD}{dN}\right)_j^i \Delta N \tag{14}$$

$$N^{i+1} = N^i + \Delta N \tag{15}$$

It should be noted that the forward difference method is used to solve Eqs. (8) and (9). It is an explicit method and the accuracy of the predicted results is relevant with the value of ΔN. A central or backward difference method would be superior. However, the results obtained by these three methods are almost identical when the value of ΔN meets the relation of $\Delta N/N_i \approx 0.01 \sim 0.02$ [21]. In this study, the value of ΔN is chosen according to this relation in order to obtain the convergent results.

(5) The algorithm repeats steps (2)–(4) for each block of cycles until the accumulated damage of any integration point reaches the critical value D_c. The number of cycles at this stage is the fretting fatigue crack initiation life. In this study, the critical value is set to 1.

4. Material and finite element model

The fretting fatigue experiment conducted by Jin and Mall [29] is used here to validate the CDM approach with consideration of wear. The material of the pads and the specimen in the experiment is Ti–6Al–4V. The method of the parameters identification for the above models is presented in the literature [27] and the parameters for Ti–6Al–4V are listed in Table 1.

Based on the symmetric configuration, one half of the fretting contact is modeled by using ABAQUS, as shown in Fig. 2. The radius of the pad is 50.8 mm and the width and one half thickness of the specimen are 6.4 and 1.9 mm, respectively. The contact between the fretting pad and the specimen is defined using the master-slave algorithm for contact between surfaces. Coulomb friction is employed based on the Lagrange multiplier contact algorithm to ensure the exact stick condition when the shear stress is less than the critical shear value. The parameter ADJUST is also used to eliminate the initial contact gap. The sliding formulation is set as Finite Sliding and the discretization method is Surface to Surface. A constant coefficient of friction COF of 0.8 is considered throughout the analyses [10,21]. It is noted that the origin of the coordinate plane is at the midpoint of the contact zone along the specimen, as the red notations indicate in Fig. 2. The element length and width on the contact surface are both 10 μm. A mesh convergence study is conducted to verify the appropriateness of the current mesh size in the contact region between the pad and the specimen. Fig. 3 shows the comparisons of finite element

Table 1
Material parameters for Ti–6Al–4V.

E (MPa)	ν	σ_y (MPa)	C_1 (MPa)	γ_1	C_2 (MPa)
11,6000	0.34	965	13,6500	1050	8100
γ_2	σ_u (MPa)	σ_{l0} (MPa)	β	$aM_0^{-\beta}$	b_1 (MPa^{-1})
45	1180	358	2.1	1.79×10^{-11}	0.0013
b_2 (MPa^{-1})	a	S(MPa)	m		
0.00055	0.75	9.9293	4.7846		

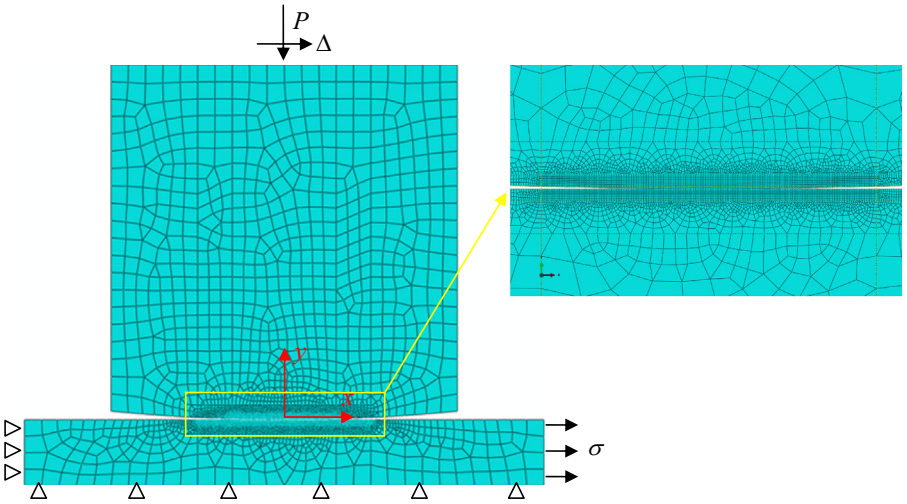

Fig. 2. Finite element model of fretting fatigue.

results of contact pressure, shear traction and σ_{xx} along the contact surface with the theoretical solutions.

The results of the contact pressure and the shear traction agree well with the theoretical results in spite of some fluctuations that appeared in the central zone of the two figures, as shown in Fig. 3 (a) and (b). The main reason for the fluctuations is the use of first-order fully integration element CPE4 which is less suitable to calculate the contact problem than the first-order reduced integration element CPE4R or incompatible mode element CPE4I in ABAQUS. Although the two types of elements, CPE4R and CPE4I, are more suitable to be used in fretting fatigue, the user subroutine UMESHMOTION to simulate the wear is not supported by them. Therefore, the element type of CPE4 is chosen in this study. Because no wear occurs in the central contact zone under the partial slip condition and the fatigue damage localizes at the edge of contact zone or the stick-slip interface which are both away from the central contact zone, the fluctuations have little effect on the predicted results. There are some deviations between the calculated result and the theoretical solution for the distribution of σ_{xx} along the contact surface, as depicted in Fig. 3(c). Similar result was also observed in the literature by Lykins et al. [3]. The error is not relevant to the mesh refinement and the contact modeling methodology. The main reason is that the elastic half-space assumption of the theoretical solution is not quite satisfied. In order to validate this opinion, the thickness of the specimen is increased from 1.9 mm to 15 mm and the contact stress in the contact zone is recalculated. The comparison between the distributions of σ_{xx} under these two cases is shown in Fig. 3(c). The result in the case of 15 mm thickness specimen agrees better with the theoretical solution.

It is worth mentioning that the dimensions of the elements in the contact zone are close to the grain size of the material Ti–6Al–4V. This is for the purpose of obtaining accurate stress results that agree well with the analytical solution. Strictly speaking, the constitutive equations and the damage evolution model based on the micromechanics [39–42] should be adopted for such small elements. McCarthy et al. [18,19] developed a micro-mechanical based methodology to predict the fretting fatigue crack nucleation life and the propagation life, in which crystal plasticity constitutive model, corresponding microstructure-sensitive fatigue parameter for crack nucleation, and the short crack propagation method are included. Sweeney et al. [43] also presented a strain-gradient crystal plasticity methodology to investigate the grain size effects on cyclic hysteresis response and LCF of CoCr alloy. However, for approximate calculations, the continuum plasticity and damage models may also be used to provide reasonable results [21,44].

As depicted in Fig. 4, a constant normal force P with a value of 208 N/mm is applied to the pad by using the Multi-Point Constraint (MPC). The axial fatigue stress σ is loaded at the right side of the specimen, which has a maximum value of 550 MPa and stress ratio of 0.03 while the in-phase relative slip amplitude Δ is applied to the pad by the MPC method.

5. Results and discussion

In the fretting fatigue, the specimen is stretched by the bulk fatigue stress and the pad moves within the range of the relative slip amplitude. When the maximum bulk fatigue stress is a constant, the relative slip amplitude determines the contact status. Table 2 lists the local relative slip amplitude and the contact status calculated under different relative slip amplitude, the value of which ranges from 20 μm to 43 μm. When the value of relative slip amplitude is greater than 32 μm, which is also greater than the maximum deformation of the material in the contact zone of the specimen, the pad moves forward compared to the specimen. The local relative slip amplitude increases with the increasing relative slip amplitude and the contact status changes from partial slip to gross sliding when the value reach 43 μm. A similar trend can be found when the relative slip amplitude decreases from 31 μm to 20 μm. The only difference is that the pad moves backward compared to the specimen.

The effects of the relative slip amplitude and wear coefficient are considered for the condition of partial slip. In this study, five relative slip amplitudes meeting the partial slip condition are imposed and three wear coefficients referenced from the literature [27,45,46] are applied, as listed in Table 3. The relative slip status between the specimen and the pad are consistent under these five relative slip amplitudes. The pad moves forward compared to the specimen, which means that the resultant shear force on the contact surface of the specimen is a positive number. In order to unveil the effect of fatigue damage, a group of simulations with zero wear coefficient are conducted as a baseline in this study, in which the wear is ignored and only the fatigue damage is considered.

One may notice that the CDM approach is used to predict the position and the life of crack initiation while the orientation and propagation of the fatigue crack are not involved. For the fretting fatigue experiments conducted by Jin and Mall [29], Madge et al.

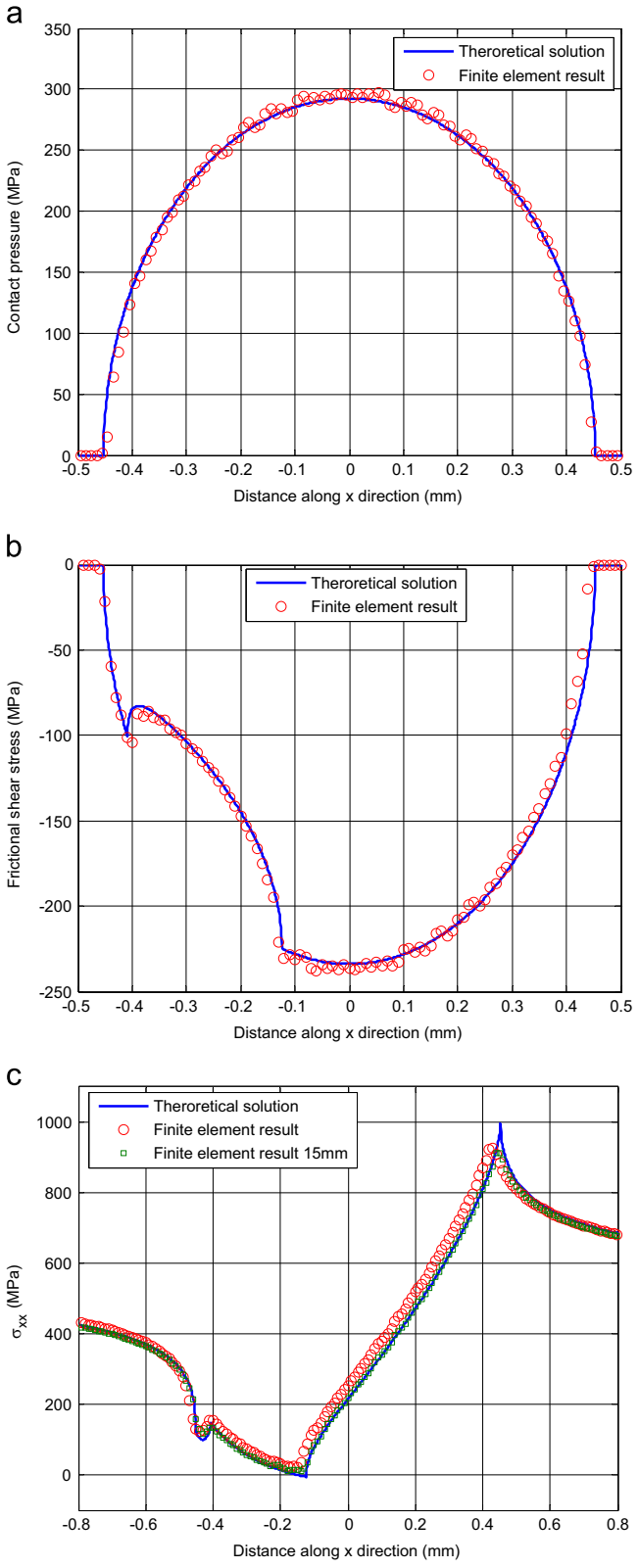

Fig. 3. Comparisons of theoretical solutions and finite element results of (a) contact pressure, (b) shear traction and (c) σ_{xx} (σ = 550 MPa, Q = −150 N/mm).

[15] used a "wear-nucleation-propagation" method to predict the fretting fatigue life and the results indicated that the propagation life is very short comparing to the nucleation life. Therefore, many researches [10,21] only consider the crack initiation life when simulating the experiments. In other words, in this study the

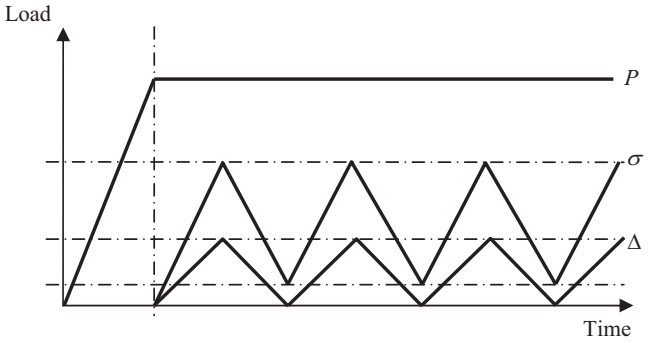

Fig. 4. Schematic view of fretting loading history.

Table 2
Calculated results under different relative slip amplitude.

Relative slip amplitude (μm)	Local relative slip amplitude (μm)	Contact condition
20	5.53	Gross sliding
23	3.42	Partial slip
25	2.88	Partial slip
27	2.42	Partial slip
30	1.66	Partial slip
31	1.42	Partial slip
32	1.26	Partial slip
34	1.79	Partial slip
36	2.36	Partial slip
38	2.99	Partial slip
40	3.67	Partial slip
43	5.17	Gross sliding

predicted results obtained using the CDM approach are comparable to the experimental results.

The predicted fretting fatigue lives are also listed in Table 3 and the comparison with the experimental results from the literature [29] is shown in Fig. 5. In addition, the predicted results in the literature [27] are plotted in Fig. 5. It is noted that the local relative slip amplitude Δ_{local} is used as the abscissa instead of the global relative slip amplitude Δ. The parameter Δ_{local} for the simulations in Table 3 can be obtained directly from the finite element analysis, as listed in Table 2. However, the local relative slip amplitude in the experiment is difficult to measure. A relationship [10] between the two relative slip amplitudes is employed for the experiment

$$\Delta_{local} = \Delta \frac{C_{COF}}{C_{rig}} \tag{16}$$

where C_{COF}, C_{rig} are constants which account for the effect on compliance of COF and rig compliance, respectively. In this study, the resulting value of C_{rig}/C_{COF} is 16 based on the data from the literature [47]. The minimum local relative slip amplitude calculated under Δ = 32 μm is greater than the minimum value in the experiments, even greater than 1 μm. From the calculated results in Table 2, one can deduce that a certain condition definitely exists corresponding to a local relative slip amplitude less than 1 μm, even being equal to zero. However, it is difficult to find this condition in the simulation. As illustrated in Fig. 5, the coupled CDM approach with consideration of wear can provide reasonable prediction of the fretting fatigue life under partial slip condition for $\phi = 2 \times 10^{-7}$ MPa^{-1}. It is noted that no constant wear coefficient for the fretting fatigue experiments conducted by Jin and Mall [29] was determined in the published literature. The value of wear coefficient, $\phi = 7.121 \times 10^{-7}$ MPa^{-1}, used by Zhang et al. [11] was obtained from the wear experiments under reciprocating sliding conditions, the relative slip amplitudes of which are greater than

Table 3
Predicted results of fretting fatigue life.

Wear coefficient ϕ	Fretting fatigue life under different relative slip amplitude				
	32 μm	34 μm	36 μm	38 μm	40 μm
0	10.7×10^4	8.1×10^4	6.4×10^4	5.2×10^4	3.7×10^4
2.9×10^{-8}MPa^{-1}[45]	19.5×10^4	13×10^4	9.1×10^4	7.3×10^4	5.2×10^4
2×10^{-7}MPa^{-1}[27]	7.6×10^4	5.7×10^4	4.6×10^4	3.7×10^4	2.7×10^4
7.121×10^{-7}MPa^{-1}[46]	4.3×10^4	2.9×10^4	1.8×10^4	1.5×10^4	1.1×10^4

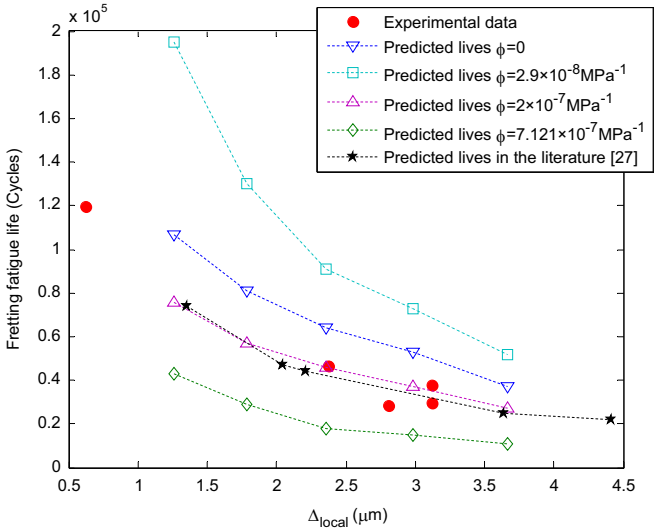

Fig. 5. Predicted fretting fatigue lives and experimental results.

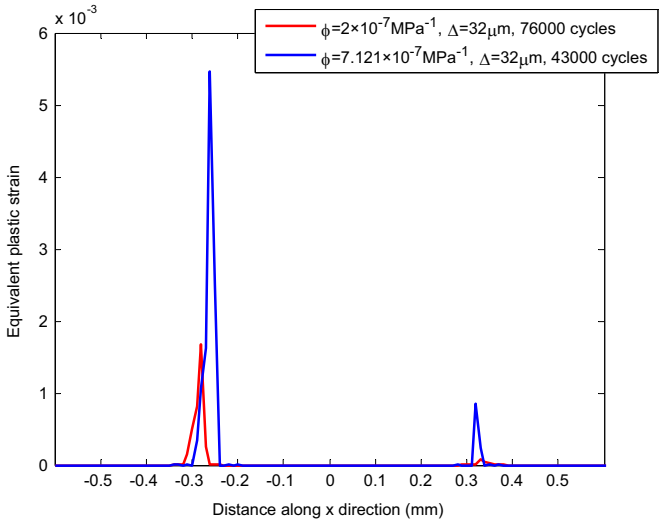

Fig. 6. Comparison between the distributions of the equivalent plastic strain along the contact surface for $\phi = 2 \times 10^{-7}$ and 7.121×10^{-7} MPa^{-1} under $\Delta = 32$ μm.

the conditions in the literature [29] significantly. The value of $\phi = 2 \times 10^{-7}$ MPa^{-1} is not from fretting wear experiments and can be considered as a reference value for the fretting fatigue experiments according to the comparison in Fig. 5.

5.1. Effect of the damage cumulative rule

Comparing the two curves for $\phi = 2 \times 10^{-7}$ MPa^{-1}, the predicted results in this study are slightly higher than that in the literature [27]. The reason is that the cumulative rate of fatigue damage is calculated by choosing the greater one in the two rates, which is less than that calculated by the sum of the two rates. As reported in [27], the equivalent plastic strain is small and the plastic damage rate calculated by Eq. (9) is about one magnitude less than the elastic damage rate given by Eq. (8). The deviation of the fretting fatigue lives predicted by the two damage cumulative rules is insignificant for the cases of $\phi = 2 \times 10^{-7}$ MPa^{-1}.

The difference between the two damage accumulation rules will be obvious for the case with a greater wear coefficient. Fig. 6 shows the comparison between the distributions of the equivalent plastic strain along the contact surface for $\phi = 2 \times 10^{-7}$and 7.121×10^{-7} MPa^{-1} under $\Delta = 32$ μm when the fretting fatigue crack initiates. When $\phi = 2 \times 10^{-7}$ MPa^{-1}, the maximum equivalent plastic strain is relatively small and the elastic damage rate is about one magnitude bigger than the plastic damage rate. With greater wear coefficient, the peak of the equivalent plastic strain is higher, as shown in Fig. 6. For $\phi = 7.121 \times 10^{-7}$ MPa^{-1}, the maximum plastic damage rate at the location of crack initiation is about 1.15×10^{-5} while the maximum value of the elastic damage rate is about 2.95×10^{-5}. If the two rates with same magnitude are summed to calculate the fatigue damage, the predicted fatigue life will be much shorter than that obtained in this study. While for $\phi = 2.9 \times 10^{-8}$ MPa^{-1}, the wear is insignificant and the plastic strain hardly occurs along the contact surface. The distribution of the equivalent plastic strain along the contact surface is not plotted in Fig. 6. The maximum plastic damage rate is much less than the elastic damage rate, which cause the results from the two different damage cumulative rules to have an insignificant difference.

5.2. Effect of relative slip amplitude

The group of simulations with zero wear coefficient is chosen to study the effect of relative slip amplitude Δ. As the value of the relative slip amplitude increases from $\Delta = 32$ μm to $\Delta = 40$ μm, the predicted fretting fatigue life decreases but the initiation position of the fretting fatigue crack remains unchanged, at the left contact edge. A qualitative explanation is that the greater relative slip amplitude results in the higher frictional tangential force Q along the contact surface. With the unchanged normal force P and axial fatigue stress σ, the increase of the tangential force Q will accelerate the initiation of the fretting fatigue crack. More detailed explanation is presented by the distributions of the axial stress component σ_{xx} and the shear traction along the contact surface, as shown in Fig. 7(a) and (b) respectively. While the distributions of contact pressure are not presented because they are identical for all the five cases due to the same normal force P. Fig. 7(a) shows that the peak value of σ_{xx} grows obviously with the increase of the relative slip amplitude. Since the peak value of the stress component σ_{xx} at the left contact edge is much higher than the other three stress components, the distribution of σ_{xx} determines the fatigue damage process. Thus, the fretting fatigue life decreases as the relative slip amplitude increases. Meanwhile, Fig. 7(b) suggests the peak value of the shear traction has a small change as the relative slip amplitude changes and the position of it is not at the left contact edge, leading to the insignificant effect on the fretting fatigue life.

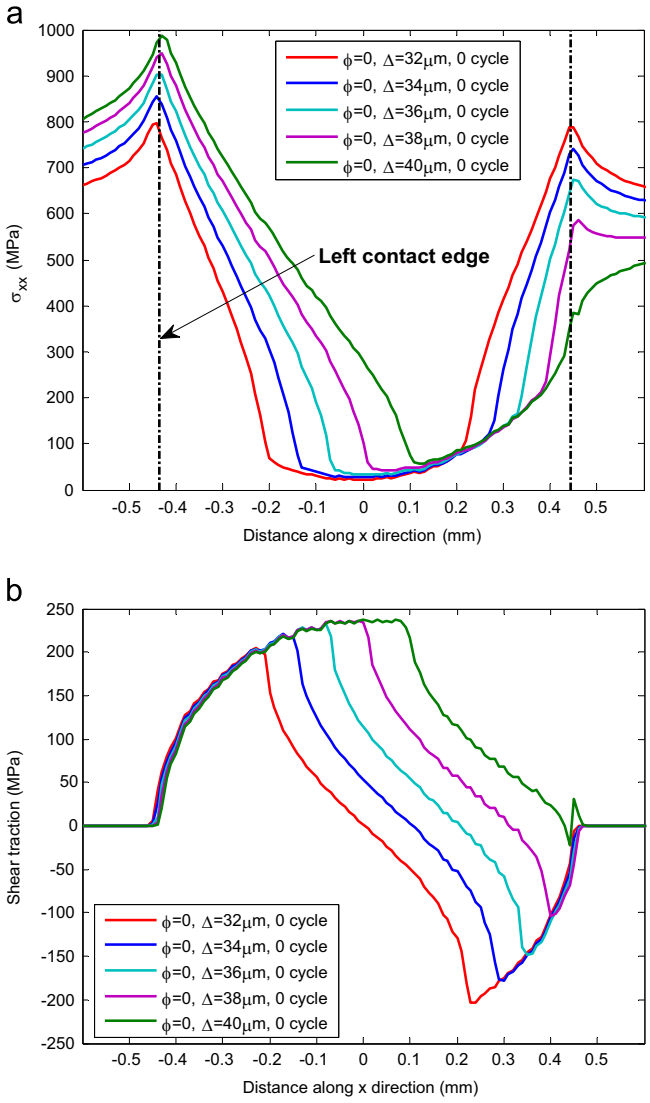

Fig. 7. Distributions of (a) σ_{xx}, (b) shear traction along the contact surface at different relative slip amplitudes.

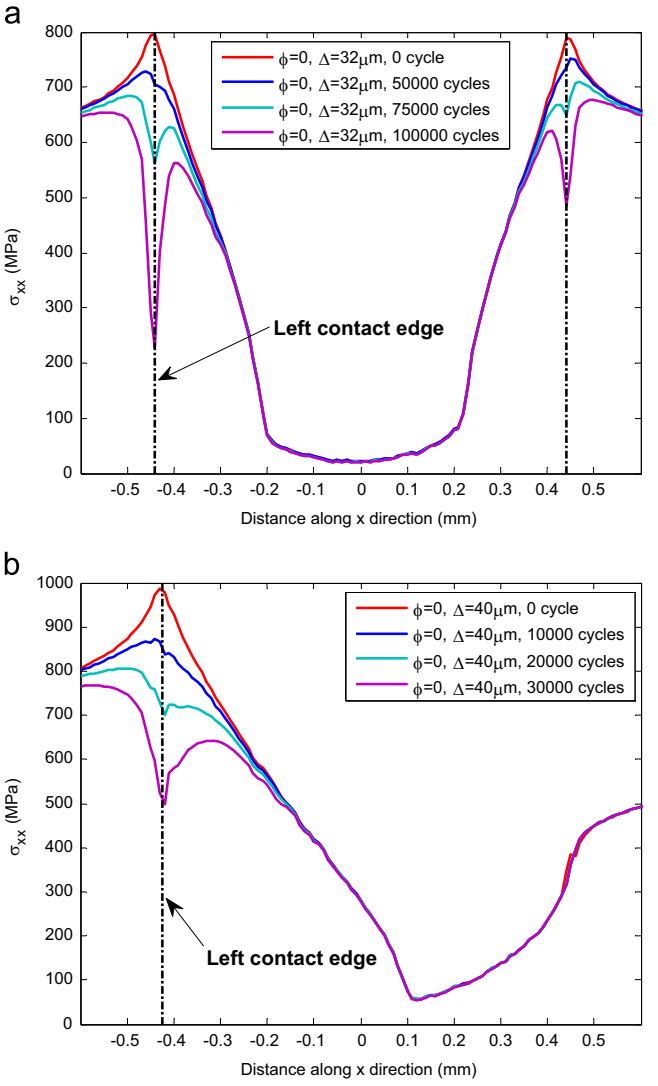

Fig. 8. Evolutions of the distribution of σ_{xx} along the contact surface for (a) $\Delta = 32$ μm and (b) 40 μm.

5.3. *Effect of fatigue damage*

The distribution of σ_{xx} changes as the number of cycles increases due to fatigue damage. This phenomenon of stress redistribution is a feature of the coupled CDM approach. In this study, a direct method is employed to study the effect of fatigue damage, instead of the comparative analysis [27]. The group of simulations with zero wear coefficient is chosen to eliminate the effect of wear. Fig. 8(a) and (b) depict the evolutions of the distribution of σ_{xx} along the contact surface for $\Delta = 32$ μm and 40 μm respectively. For the case of $\Delta = 32$ μm, fatigue damage concentrates on two contact edges, $x = \pm 0.44$ mm, and fatigue crack finally occurs at the left contact edge. As the number of cycles increases, the value of σ_{xx} decreases at the damage zone. The decline is more obvious at the left contact edge due to worse fatigue damage. For the case of $\Delta = 40$ μm, fatigue damage just concentrates on the left contact edge, and the value of σ_{xx} decreases rapidly with the increasing number of cycles. Finally, fatigue crack initiates at the position of $x = -0.43$ mm. The difference between the two cases mainly comes from the different distributions of σ_{xx}, as shown in Fig. 7(a).

Meanwhile, fatigue damage has insignificant effect on the distributions of the contact pressure and shear traction. Fig. 9(a) and (b) depict the evolution of the contact pressure along the contact surface for $\Delta = 32$ μm and 40 μm respectively. The curves in Fig. 9 (a) and (b) are almost identical except that little variation occurs at the zone near the left contact edge. Similar trend is obtained for the evolution of the shear traction. Some fluctuations occur in the central contact zone, which are away from the contact edges.

Fatigue damage is coupled into the Chaboche plasticity model, which will weaken the mechanical performance of the material under the contact surface. Due to the stress concentration, the fatigue damage is localized at the contact edges. Fig. 10 shows the distributions of fatigue damage along the contact surface for $\Delta = 32$ μm and 40 μm when the fatigue crack initiates. The material properties of several elements near the contact edges are affected by the fatigue damage but these influenced elements constitute only a very small part of the contact, which affects the whole contact stiffness insignificantly. Therefore, no obvious effect on the contact calculation, including the evolution of contact pressure and shear traction, is found. While the stress component σ_{xx} is related to the material properties of the element directly, the effect on σ_{xx} is significant.

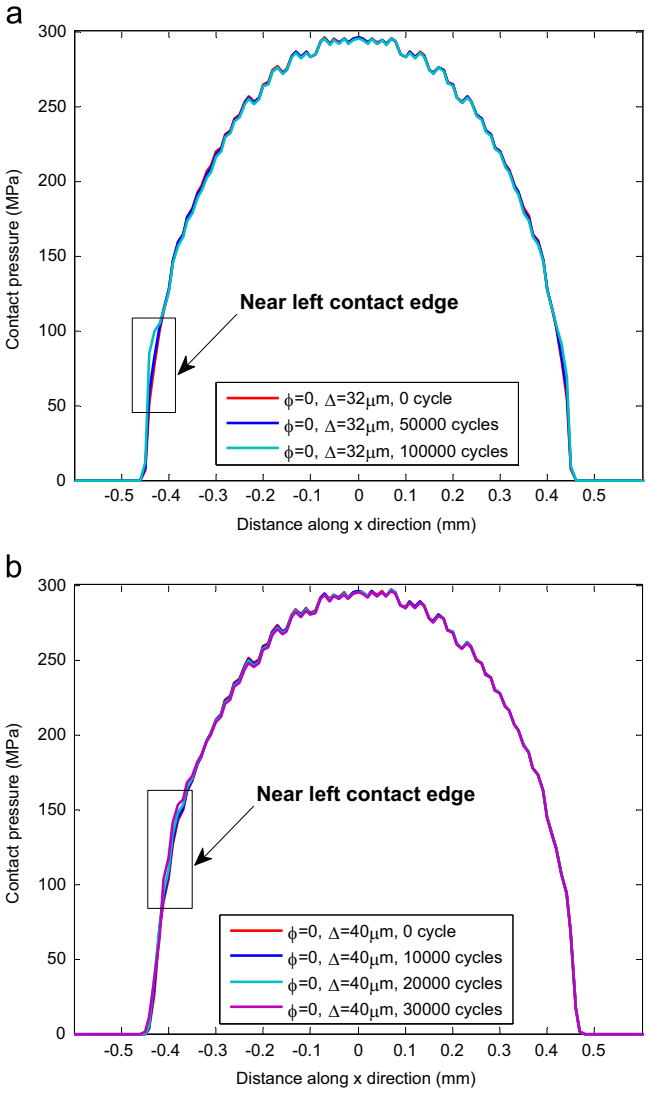

Fig. 9. Evolutions of the distribution of contact pressure along the contact surface for (a) $\Delta = 32\ \mu m$ and (b) 40 μm.

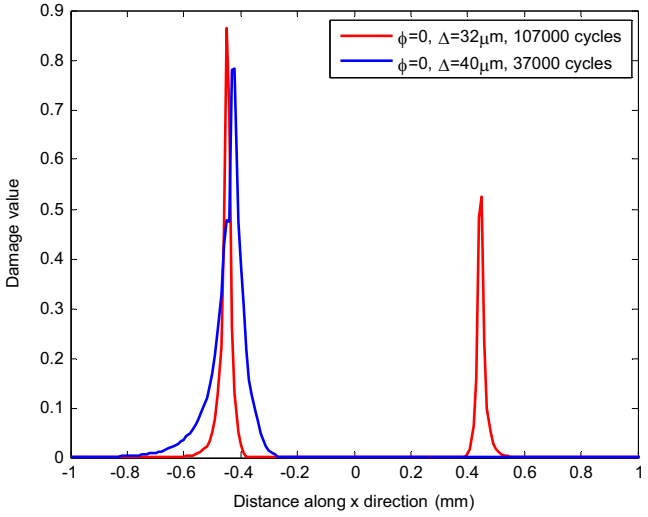

Fig. 10. Distributions of fatigue damage along the contact surface for $\Delta = 32\ \mu m$ and 40 μm when the fatigue crack initiates.

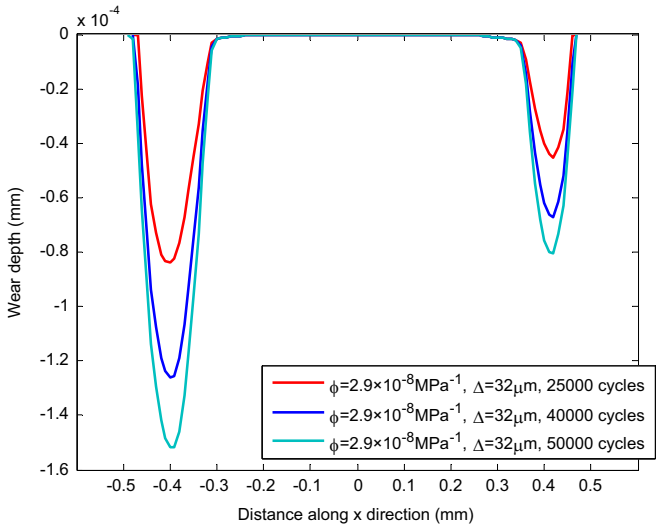

Fig. 11. Evolution of wear scar along the contact surface for $\Delta = 32\ \mu m$ and $\phi = 2.9 \times 10^{-8}\ MPa^{-1}$ without consideration of fatigue damage.

5.4. Effect of wear coefficient

Based on the principle of analysis for a single factor, the effect of wear coefficient is investigated by the comparisons under the same relative slip amplitude. In order to separate the effect of wear, additional simulations are conducted based on the numerical algorithm in Section 4 by ignoring step (4) which is conducted in order to calculate the fatigue damage.

For the case of $\Delta = 32\ \mu m$, Fig. 11 depicts the evolution of wear scar along the contact surface for $\phi = 2.9 \times 10^{-8}\ MPa^{-1}$. Wear occurs at two slip zones and the wear depth increases with the increasing number of cycles. As the result of the evolution of contact geometry, the distributions of contact stresses and subsurface stress vary from cycle to cycle. Fig. 12 shows the evolution of σ_{xx} along the contact surface. The value of σ_{xx} at the left contact edge $x = -0.44$ mm drops due to the removal of material while its value near the left stick-slip interface $x = -0.31$ mm increases slightly. The peak value is always at the left contact edge before 50,000 cycles. For the aim of investigating the effect of wear coefficient, the investigators also carry out the wear simulation for the case of $\phi = 2 \times 10^{-7}\ MPa^{-1}$. Fig. 13 illustrates the evolution of σ_{xx} along the contact surface. Under the higher wear coefficient, the effect of wear on the stress evolution is more evident. The same trends of the evolution at the left contact edge and the left stick-slip interface are found by comparing Figs. 12 and 13. However, the stress value at the left stick-slip interface increases significantly for $\phi = 2 \times 10^{-7}\ MPa^{-1}$. The peak moves from the left contact edge to the left stick-slip interface as the number of cycles increases to 20,000 cycles.

The effect of wear coefficient can be summarized in that the value of stress component σ_{xx} decreases at the left contact edge but increases at the left stick-slip interface. The increment is more significant with greater wear coefficient, which makes the left stick-slip interface as a critical position of the fatigue crack initiation. Two main reasons can be concluded for the different influence at the left stick-slip interface for the two wear coefficients: (1) The wear scar at the two slip zones is deeper with greater wear coefficient, which weakens the loading capacity of the slip zones. The loading condition at the central stick zone grows more severe. (2) The deeper wear scar results in more drastic change of the contact geometry at the left stick-slip interface.

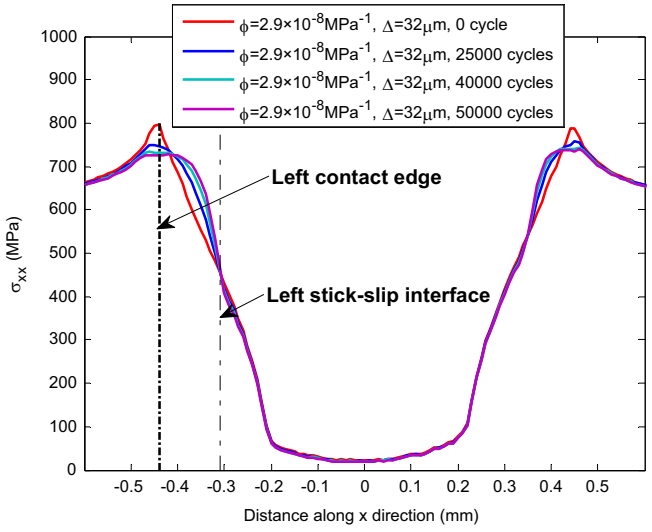

Fig. 12. Evolution of σ_{xx} along the contact surface for $\Delta = 32\ \mu m$ and $\phi = 2.9 \times 10^{-8}\ MPa^{-1}$ without consideration of fatigue damage.

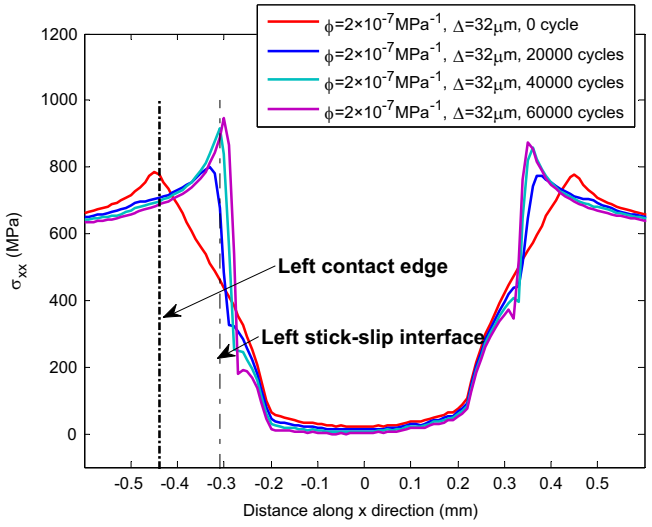

Fig. 13. Evolution of σ_{xx} along the contact surface for $\Delta = 32\ \mu m$ and $\phi = 2 \times 10^{-7}\ MPa^{-1}$ without consideration of fatigue damage.

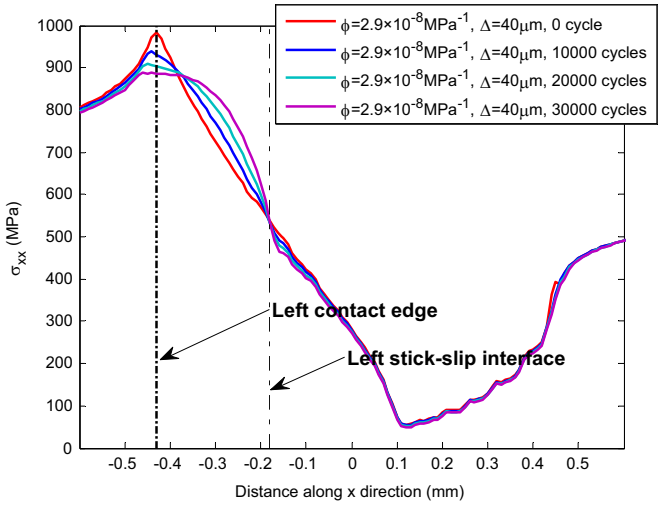

Fig. 14. Evolutions of σ_{xx} along the contact surface for $\Delta = 40\ \mu m$ and $\phi = 2.9 \times 10^{-8}\ MPa^{-1}$ without consideration of fatigue damage.

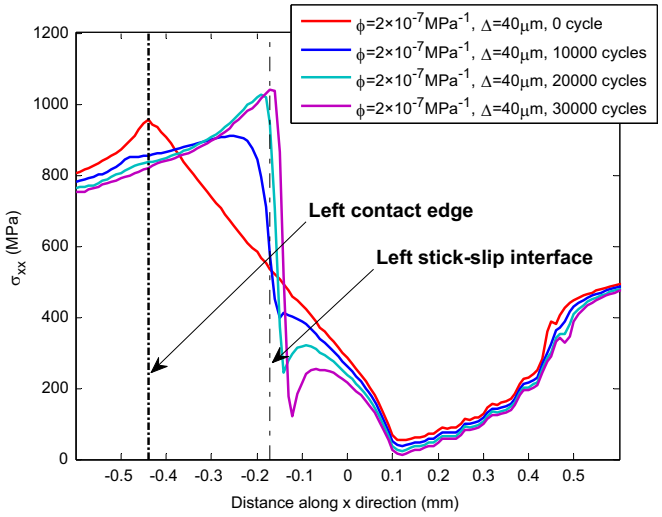

Fig. 15. Evolutions of σ_{xx} along the contact surface for $\Delta = 40\ \mu m$ and $\phi = 2 \times 10^{-7}\ MPa^{-1}$ respectively without consideration of fatigue damage.

Figs. 14 and 15 show the evolutions of σ_{xx} along the contact surface for $\Delta = 40\ \mu m$ and $\phi = 2.9 \times 10^{-8}\ MPa^{-1}$, and $\Delta = 40\ \mu m$ and $\phi = 2 \times 10^{-7}\ MPa^{-1}$ respectively. A similar tendency to the cases of $\Delta = 32\ \mu m$ is observed for the evolution of σ_{xx} for the cases of $\Delta = 40\ \mu m$. The position of the left stick-slip interface moves to $x = -0.17$ mm but no obvious moving of the right stick-slip interface is observed.

The authors also investigate the effect of wear coefficient on the fretting fatigue life when the fatigue damage and wear are both considered in the coupled CDM approach. The fatigue crack occurs at the left contact edge for $\phi = 2.9 \times 10^{-8}\ MPa^{-1}$, which is the same as the baseline simulation with zero wear coefficient. Although the stress value at the left stick-slip interface increases, the maximum value is still at the left contact edge. The rate of fatigue damage accumulation is higher at the left contact edge than that at the left stick-slip interface. Compared to the baseline cases with zero wear coefficient, the predicted fretting fatigue lives are larger for $\phi = 2.9 \times 10^{-8}\ MPa^{-1}$, as shown in Fig. 5. The reason is that the stresses at the left contact edge are reduced due to wear. However, the fatigue crack initiates at the left stick-slip interface for $\phi = 2 \times 10^{-7}$ and $7.121 \times 10^{-7}\ MPa^{-1}$. Fig. 16 shows the distribution of fatigue damage along the contact surface for $\Delta = 32\ \mu m$ and $\phi = 2 \times 10^{-7}\ MPa^{-1}$ when the fatigue crack initiates. Although the fretting fatigue crack occurs finally at the left stick-slip interface, the peak of σ_{xx} is at the left contact edge at the beginning of the simulation. Therefore, it is necessary to investigate the accumulation of the fatigue damage at the two positions, the left contact edge and the left stick-slip interface. Fig. 17 shows the accumulations of the fatigue damage at the two positions for $\Delta = 32\ \mu m$ and $\phi = 2 \times 10^{-7}\ MPa^{-1}$. At the beginning of the simulation, the fatigue damage at the left contact edge is greater than that at the left stick-slip interface. As the number of cycles increases, the stresses at the left stick-slip interface increases significantly due to wear. Therefore, the fatigue damage at the left stick-slip interface exceeds that at the left contact edge after certain cycles. The predicted fretting fatigue lives for $\phi = 2 \times 10^{-7}$ and $7.121 \times 10^{-7}\ MPa^{-1}$ are shorter than the baseline results with zero wear coefficient.

The above results indicate the effect of the wear coefficient on the fretting fatigue life is non-monotonic. A small wear coefficient may prolong the fatigue life compared to the baseline case. The fatigue life then decreases with the further increase of wear coefficient. This tendency is attributed to the complex variation of

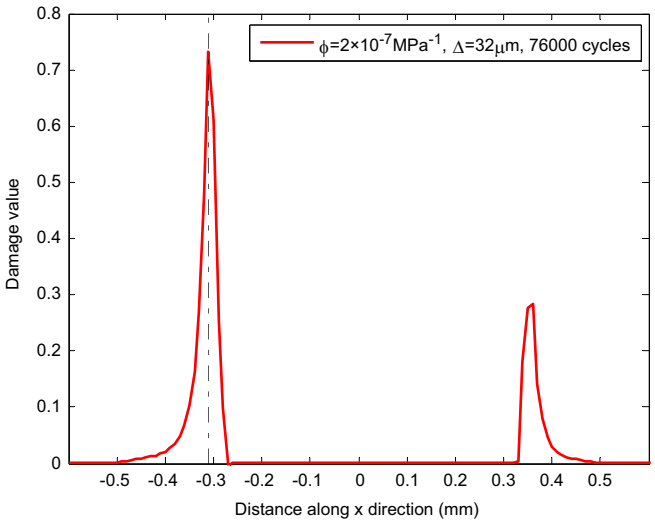

Fig. 16. Distribution of fatigue damage along the contact surface for $\Delta = 32$ μm and $\phi = 2 \times 10^{-7}$ MPa^{-1} when the fatigue crack initiates.

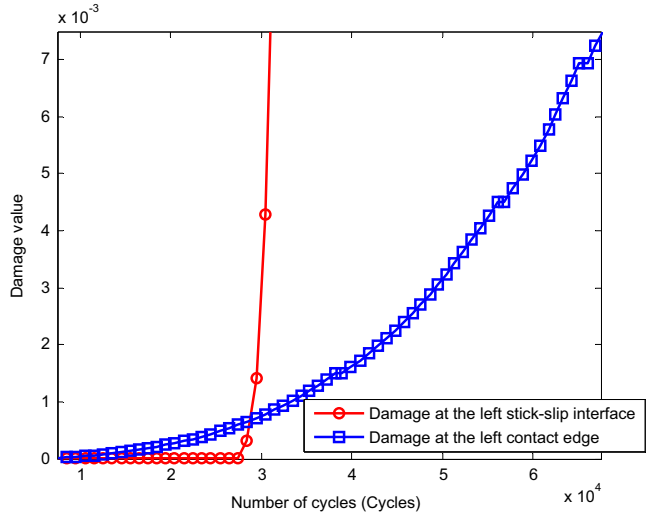

Fig. 17. Accumulations of the fatigue damage at the two positions for $\Delta = 32$ μm and $\phi = 2 \times 10^{-7}$ MPa^{-1}.

distribution of σ_{xx} which can influence the fatigue damage accumulation and critical position simultaneously.

5.5. Combined effects of fatigue damage and wear

The simulations for $\phi = 2 \times 10^{-7}$ MPa^{-1} in Table 3 are chosen to investigate the combined effects of the fatigue and wear. Fig. 18 depicts the evolution of the distribution of σ_{xx} along the contact surface for $\Delta = 32$ μm and $\phi = 2 \times 10^{-7}$ MPa^{-1}. Different relationship between the fatigue damage and wear can be obtained at the two critical positions. The fatigue damage and wear combine to decrease the value of σ_{xx} at the left contact edge. The stress component drops at the left contact edge as the number of cycles increases to 60,000 cycles, as shown in Fig. 18. However, the relationship between the fatigue damage and wear is competitive at the left stick-slip interface. The fatigue damage decreases the value of the stress component while the wear increases it. At the beginning of the simulations, the value of the fatigue damage is small and the effect of wear is predominant. Whereafter, the effect of fatigue damage becomes significant compared to the effect of

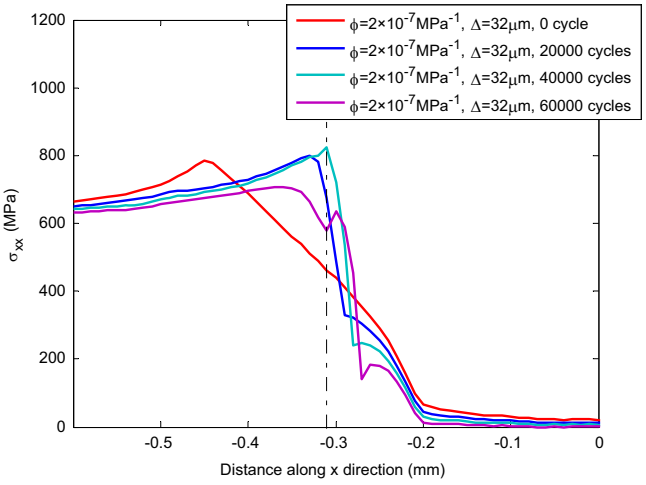

Fig. 18. Evolution of the distribution of σ_{xx} along the contact surface for $\Delta = 32$ μm and $\phi = 2 \times 10^{-7}$ MPa^{-1}.

wear as the fatigue damage increases and as the number of cycles increase. Therefore, the combined effects increase first and then decrease the value of σ_{xx} with the increase of the number of cycles. This combined and competitive relationship also exists in the simulations for $\phi = 2.9 \times 10^{-8}$ and 7.121×10^{-7} MPa^{-1}.

However, whichever one of the two actions plays a crucial role has a close relation with the value of the wear coefficient. In this study, the combined effect is important for the prediction of fretting fatigue life under $\phi = 2.9 \times 10^{-8}$ MPa^{-1} because the fatigue crack initiates at the left contact edge. In the case of $\phi = 2 \times 10^{-7}$and 7.121×10^{-7} MPa^{-1}, the competition at the left stick-slip interface is more significant, which leads to the initiation of the fatigue crack.

6. Conclusions

In this study, the effects of the relative slip amplitude and wear coefficient to the fretting fatigue behavior are evaluated in the condition of partial slip based on the improved CDM approach. Some key findings can be concluded as follows:

- The improved fatigue damage accumulation rule can predict a more reasonable and accurate damage process.
- The stress component σ_{xx} with higher peak value is more significant in the fretting fatigue compared to the other three stress components. It almost determines the fretting fatigue behavior.
- The fretting fatigue life decreases with the increase of the relative slip amplitude. This is because the peak value of σ_{xx} increases as the relative slip amplitude increases, which accelerates the initiation of fretting fatigue crack.
- The fatigue damage is restricted to a small zone along the contact surface of the specimen, which obviously decreases the value of σ_{xx} but has insignificant effect on the contact pressure and shear traction.
- The influence of wear on the contact stress and the fretting fatigue life cannot be ignored. The effect of the wear coefficient is non-monotonic. This reason can be attributed to the complex variation of the distribution of σ_{xx}.
- The combination and competition between fatigue damage and wear is presented and evaluated. Whichever one of the two actions plays a crucial role it accordingly has a close relation with the value of the wear coefficient.

Acknowledgments

Financial support by National Natural Science Foundation of China (11002010) is gratefully acknowledged. The authors also appreciate the support of the Computational Solid Mechanics Laboratory at Louisiana State University.

References

[1] M.P. Szolwinski, T.N. Farris, Mechanics of fretting crack formation, Wear 198 (1996) 93–107.
[2] M.P. Szolwinski, T.N. Farris, Observation, analysis and prediction of fretting fatigue in 2024-T351 aluminum alloy, Wear 221 (1998) 24–36.
[3] C.D. Lykins, S. Mall, V. Jain, An evaluation of parameters for predicting fretting fatigue crack initiation, Int. J. Fatigue 22 (2000) 703–716.
[4] J.A. Araújo, D. Nowell, The effect of rapidly varying contact stress fields on fretting fatigue, Int. J. Fatigue 24 (2002) 763–775.
[5] J. Vázquez, C. Navarro, J. Domínguez, Analysis of the effect of a textured surface on fretting fatigue, Wear 305 (2013) 23–35.
[6] J.F. Archard, Contact and rubbing of flat surfaces, J. Appl. Phys. 24 (1953) 981–988.
[7] S. Fouvry, T. Liskiewicz, P.H. Kapsa, S. Hannel, E. Sauger, An energy description of wear mechanisms and its applications to oscillating sliding contacts, Wear 255 (2003) 287–298.
[8] B. Zeise, R. Liebich, M. Prölß, Simulation of fretting wear evolution for fatigue endurance limit estimation of assemblies, Wear 316 (2014) 49–57.
[9] J.J. Madge, S.B. Leen, P.H. Shipway, The critical role of fretting wear in the analysis of fretting fatigue, Wear 263 (2007) 542–551.
[10] J.J. Madge, S.B. Leen, I.R. McColl, P.H. Shipway, Contact-evolution based prediction of fretting fatigue life: effect of slip amplitude, Wear 262 (2007) 1159–1170.
[11] T. Zhang, P.E. McHugh, S.B. Leen, Computational study on the effect of contact geometry on fretting behavior, Wear 271 (2011) 1462–1480.
[12] S. Basseville, G. Cailletaud, An evaluation of the competition between wear and crack initiation in fretting conditions for Ti–6Al–4V alloy, Wear 328–329 (2015) 443–455.
[13] C. Gandiolle, S. Fouvry, FEM modeling of crack nucleation and crack propagation fretting fatigue maps: plasticity effect, Wear 330–331 (2015) 136–144.
[14] S. Garcin, S. Fouvry, S. Heredia, A. FEM, fretting map modeling: effect of surface wear on crack nucleation, Wear 330–331 (2015) 145–159.
[15] J.J. Madge, S.B. Leen, P.H. Shipway, A combined wear and crack nucleation–propagation methodology for fretting fatigue prediction, Int. J. Fatigue 30 (2008) 1509–1528.
[16] R. Hojjati-Talemi, M.A. Wahab, E. Giner, M. Sabsabi, Numerical estimation of fretting fatigue lifetime: using damage and fracture mechanics, Tribol. Lett. 52 (2013) 11–25.
[17] R. Hojjati-Talemi, M.A. Wahab, J. De Pauw, P. De Baets, Prediction of fretting fatigue crack initiation and propagation lifetime for cylindrical contact configuration, Tribol. Int. 76 (2014) 73–91.
[18] O.J. McCarthy, J.P. McGarry, S.B. Leen, Microstructure-sensitive prediction and experimental validation of fretting fatigue, Wear 305 (2013) 100–114.
[19] O.J. McCarthy, J.P. McGarry, S.B. Leen, The effect of grain orientation on fretting fatigue plasticity and life prediction, Tribol. Int. 76 (2014) 100–115.
[20] R. Hojjati-Talemi, M.A. Wahab, Fretting fatigue crack initiation lifetime predictor: using damage mechanics approach, Tribol. Int. 60 (2013) 176–186.
[21] T. Zhang, P.E. McHugh, S.B. Leen, Finite element implementation of multiaxial continuum damage mechanics for plain and fretting fatigue, Int. J. Fatigue 44 (2012) 260–272.
[22] A.A. Walvekar, B.D. Leonard, F. Sadeghi, B. Jalalahmadi, N. Bolander, An experimental study and fatigue damage model for fretting fatigue, Tribol. Int. 79 (2014) 183–196.
[23] O. Jin, S. Mall, Effects of independent pad displacement on fretting fatigue behavior of Ti–6Al–4V, Wear 253 (2002) 585–596.
[24] O. Jin, S. Mall, Influence of contact configuration on fretting fatigue behavior of Ti–6Al–4V under independent pad displacement condition, Int. J. Fatigue 24 (2002) 1243–1253.
[25] J. Ding, G. Bandak, S.B. Leen, E.J. Williams, P.H. Shipway, Experimental characterization and numerical simulation of contact evolution effect on fretting crack nucleation for Ti–6Al–4V, Tribol. Int. 42 (2009) 1651–1662.
[26] A.L. Mohd Tobi, J. Ding, G. Bandak, S.B. Leen, P.H. Shipway, A study on the interaction between fretting wear and cyclic plasticity for Ti–6Al–4V, Wear 267 (2009) 270–282.
[27] F. Shen, W.P. Hu, Q.C. Meng, A damage mechanics approach to fretting fatigue life prediction with consideration of elastic–plastic damage model and wear, Tribol. Int. 82 (2015) 176–190.
[28] F. Shen, G.Z. Voyiadjis, W.P. Hu, Q.C. Meng, Analysis on the fatigue damage evolution of notched specimens with consideration of cyclic plasticity, Fatigue Fract. Eng. Mater. Struct. (2015), http://dx.doi.org/10.1111/ffe.12299.
[29] O. Jin, S. Mall, Effects of slip on fretting behavior: experiments and analysis, Wear 256 (2004) 671–684.
[30] J. Ding, S.B. Leen, I.R. McColl, The effect of slip regime on fretting wear-induced stress evolution, Int. J. Fatigue 26 (2004) 521–531.
[31] C.L. Chow, J. Wang, An anisotropic theory of continuum damage mechanics for ductile fracture, Eng. Fract. Mech. 27 (5) (1987) 547–558.
[32] G.Z. Voyiadjis, B. Deliktas, A coupled anisotropic damage model for the inelastic response of composite materials, Comput. Methods Appl. Mech. Eng. 183 (3) (2000) 159–199.
[33] L.L. Sun, W.P. Hu, M. Zhang, Q.C. Meng, An anisotropic damage model based on microstructure of boom–panel for the fatigue life prediction of structural components, Fatigue Fract. Eng. Mater. Struct. 37 (11) (2014) 1186–1196.
[34] J.L. Chaboche, Constitutive equations for cyclic plasticity and cyclic viscoplasticity, Int. J. Plast. 5 (1989) 247–302.
[35] J. Lemaitre, D. Rodrigue, Engineering Damage Mechanics, Springer, New York, 2005.
[36] J. Lemaitre, J.L. Chaboche, Mechanics of Solid Materials, Cambridge University Press, United Kingdom, 1994.
[37] A.K. Marmi, A.M. Habraken, L. Duchene, Multiaxial fatigue damage modeling at macro scale of Ti–6Al–4V alloy, Int. J. Fatigue 31 (2009) 2031–2040.
[38] ABAQUS/Standard version 6.10, User manual. Hibbit Karlsson and Sorensen Inc, Rhode Island, USA, 2010.
[39] G.Z. Voyiadjis, Damage Mechanics and Micromechanics of Localized Fracture Phenomena in Inelastic Solids, Springer, New York, 2012.
[40] G.Z. Voyiadjis, Handbook of Damage Mechanics Nano to Macro Scale for Materials and Structures, Springer, New York, 2014.
[41] A. Glema, T. Lodygowski, W. Sumelka, P. Perzyna, The numerical analysis of the intrinsic anisotropic microdamage evolution in elasto-viscoplastic solids, Int. J. Damage Mech. 18 (2009) 205–231.
[42] T. Łodygowski, P. Perzyna, Numerical modelling of localized fracture of inelastic solids in dynamic loading processes, Int. J. Numer. Methods Eng. 40 (1997) 4137–4158.
[43] C.A. Sweeney, B. O'Brien, F.P.E. Dunne, P.E. McHugh, S.B. Leen, Strain-gradient modelling of grain size effects on fatigue of CoCr alloy, Acta Mater. 78 (2014) 341–353.
[44] A. Ghosh, B.D. Leonard, F. Sadeghi, A stress based damage mechanics model to simulate fretting wear of Hertzian line contact in partial slip, Wear 307 (2013) 87–99.
[45] V. Fridrici, S. Fouvry, P.H. Kapsa, Effect of shot peening on the fretting wear of Ti–6Al–4V, Wear 250 (2001) 642–649.
[46] R.S. Magaziner, V.K. Jain, S. Mall, Wear characterization of Ti–6Al–4V under fretting-reciprocating sliding conditions, Wear 264 (2008) 1002–1014.
[47] V. Sabelkin, S. Mall, Investigation into relative slip during fretting fatigue under partial slip contact condition, Fatigue Fract. Eng. Mater. Struct. 28 (2005) 809–824.